Progress in Physics of Applied Materials 7 (2027), Serial Number 14, 1-8

Semnan University

Progress in Physics of Applied Materials

journal homepage: https://ppam.semnan.ac.ir/

Structural and Optical Properties of NiO-Doped WO_3 Thin Films Prepared by Pulsed Laser Deposition

Batool Faydhe Al-Azzawi [a], Hussein J. Abdul Karim [a], Mohammed A. Salman [b*], Mustafa E. Hammadi [c], Laith I. Khalil[d]

[a]*Department of Information and Communication Technology, Polytechnic College for Engineering Disciplines, Middle Technical University (MTU), Baghdad, 10001, Iraq*
[b]*Remote Sensing Unit, College of Science, University of Baghdad, Baghdad, 10001, Iraq*
[c]*Department of Remote Sensing, College of Science, University of Baghdad, Baghdad, 10001, Iraq*
[d]*Department of Medical Physics, College of Science, Al-Farahidi University, Baghdad, 10001, Iraq*

ARTICLE INFO

Article history:
Received: 1 January 2026
Revised: 11 May 2026
Accepted: 13 May 2026
Published online: 7 June 2026

Keywords:
$(WO_3)_{1-x}(NiO)_x$ Films;
Pulsed Laser Deposition Technique;
Structural Optical Properties.

ABSTRACT

This study investigates the effect of NiO incorporation on the structural and optical properties of WO_3 thin films deposited on glass substrates using pulsed laser deposition (PLD). The NiO concentration is varied (0.2,0.4 and 0.6 wt.%) while maintaining identical deposition conditions to isolate its intrinsic influence. The X-ray diffraction (XRD) analysis of the films indicates a monoclinic structure, with the shift in peaks suggesting lattice distortion due to higher amount of NiO Fourier transform infrared (FTIR) spectra show that the W–O–W and Ni–O vibrational modes are in agreement with the successful incorporation of NiO in WO_3. Optical measurements show a significant drop in transmittance from 85.59% to 24.39% at 500 nm along with increased absorption in the visible region. The optical band gap diminishes from 3.30 eV to 3.00 eV with increasing NiO concentration, owing to defect-induced localized states and structural changes. The film containing 0.6 wt.% NiO possesses high structural disorder and multiphase characteristics leading to strong band gap narrowing and strong optical absorption. The results indicate that the regulated incorporation of NiO may provide a useful strategy for tuning the structural and optical behaviour of WO_3 thin films.

1. Introduction

The thin films and nanostructured materials play a crucial role in modern technologies as electronic, photonic, and smart systems getting much smaller and require even better performance [1]. Applications of microelectronics, optoelectronic devices, sensors, and upcoming hardware platforms show that the efficiency, speed, and stability of devices greatly depend on the properties of the active materials at the nanoscale [2,3].

Semiconducting metal oxides play a central role in thin-film technologies due to their multifunctionality, chemical stability, and tunable physical properties [4]. Tungsten trioxide (WO_3) is an n-type semiconductor with a band gap typically reported in the range of 2.6–3.3 eV, depending on its phase, crystallinity, and nanostructure. WO_3 is particularly attractive because of its chemical stability, low cost, and sensitivity to structural modification, which enable tuning of its optical and electronic properties [5]. Nickel oxide (NiO) is a wide-band-gap p-type semiconductor that has optical absorption and stability complementary to WO_3. Thus, NiO can be a supporting modifier of WO_3-based thin films [6].

Recent research has investigated the incorporation of NiO into thin WO_3 films. Changes in the transmittance and

* Corresponding author.
E-mail address: mohammed.abd.s@sc.uobaghdad.edu.iq

Cite this article as:

Al-Azzawi, B.F., Abdul Karim, H.J., Salman, M.A., Hammadi, M.E. and Khalil. L.I., 2027. Structural and Optical Properties of NiO-Doped WO_3 Thin Films Prepared by Pulsed Laser Deposition. *Progress in Physics of Applied Materials*, *7*(1), pp.1-8. DOI: 10.22075/ppam.2026.40444.1204

crystallinity of NiO–WO_3 thin films deposited by pulsed laser deposition were reported by Maktoof and Mohammed in the presence of Au [7]. The optical behavior of WO_3 can be modified by composite modification, however, it is difficult to ascertain the inherent influence of NiO on the WO_3 lattice for the simultaneous presence of NiO and Au. Further, the amorphous nature of the reported films prevented establishing clear correlations amongst composition, crystallinity, and optical response. Due to this, the impact of NiO modification on WO_3 thin films may be known, however, the effect of NiO concentration only on crystallite size, surface morphology, and optical properties under constant deposition process is not known .

This study presents WO_3 thin films with different weights of NiO on glass substrates prepared by pulsed laser deposition technique at room temperature. To examine how the concentration of NiO affect the films' properties, all the deposition conditions except the NiO content were kept constant. The evaluation of the films' structural, morphological, and optical properties was carried out with the help of X-ray diffraction (XRD), atomic force microscopy (AFM), Fourier transform infrared (FTIR) spectroscopy, and UV–visible spectroscopy techniques. The purpose of this study is to analyze the relationship between composition, structure, and optical properties of WO_3-based films. This work will provide vital information that will enable the utilization of such devices in advanced electronic and optoelectronic devices. This research stands out because the NiO concentrations were evaluated under the same preparation conditions. Thus, this allows interpretation of the actions of NiO without disturbance of any other modifying factors. As a result, this approach allows for a precise and straightforward connection between composition, structure, and optical properties.

2. Experimental procedures and details

Using high-purity precursor powders, we prepared WO_3 thin film composite targets containing nickel oxide (NiO) at concentrations of 0.2, 0.4, and 0.6 wt.%. To ensure uniformity in the precursor powders, they were ground in an agate mortar for ~10 min. Subsequently, the powders obtained after drying were compacted into pellet form in the form of circular pellets having diameter of 1 cm and thickness of 0.2 cm using hydraulic press at an applied pressure of 5 tons for 10 min. Afterwards, the pellets were sintered at 700 °C for 1 h followed by cooling to room temperature naturally.

The $(WO_3)_{1-x}(NiO)_x$ thin films were deposited on the glass substrate of size 2.5 × 7.5 cm^2 by pulsed laser deposition (PLD) using the as-sintered pellets as ablation targets. A vacuum chamber was employed in order to minimize contamination of the films, which were allowed to grow at room temperature around a base pressure of 3 × 10^{-3} mbar. The PLD system utilized an Nd:YAG laser that was Q-switched, with a light wavelength of 1,064 nm, pulse energy of 600 mJ, and a repetition rate of 6 Hz [7]. A total of 200 laser pulses were applied during deposition. The optical window of the chamber allowed the laser beam to enter and impinge onto the target at an angle of 45 degrees from the surface normal. A fixed distance between a target and substrate was maintained, while the target was continuously rotated to enhance ablation uniformity and film homogeneity. The effective mass composition of the deposited $(WO_3)_{1-x}(NiO)_x$ thin films was estimated using the relation as given in Eq. (1):

$$W(WO_3)_{1-x}(NiO)_x = MWO_{3(1-x)} + MNiO_{(x)} \quad (1)$$

where $M_{WO_3} = 231.84\ g.\ mol^{-1}$ and $M_{NiO} = 74.69\ g.mol^{-1}$ denote the molar masses of tungsten oxide and nickel oxide, respectively. The parameter x represents the weight percentage of NiO, taking values of 0.2, 0.4, and 0.6 wt.%.

The phase constitution and crystal arrangement of the synthesized thin films were determined through X-ray diffraction (XRD) analysis using a SHIMADZU 6000 diffractometer. The surface topography, including texture and roughness, was examined by atomic force microscopy (AFM) with a CSPM-AA3000 system operating in micro-imaging mode.

Moreover, Fourier transform infrared (FTIR) spectroscopy was employed to investigate the vibrational modes of the films within the spectral interval of 500–4000 cm^{-1}, utilizing a SHIMADZU FTIR-8400S instrument. In addition, the optical characteristics of the deposited thin films were evaluated by ultraviolet–visible (UV–Vis) spectroscopy over a wavelength range of 300–1100 nm. Figure 1 demonstrates the schematic of the experimental pulsed laser deposition setup used for thin-film growth in the present investigation.

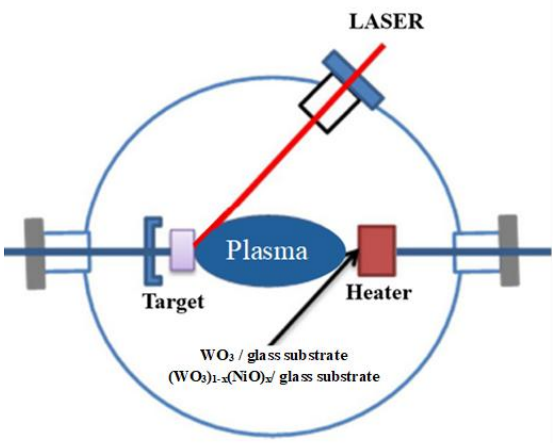

Fig. 1. Diagrammatic illustration of the experimental pulsed laser deposition setup used for thin-film growth.

3. Results and Discussion

3.1. X-ray Diffraction (XRD)

The crystal structure and phase composition of the $(WO_3)_{1-x}(NiO)_x$ thin films are examined using X-ray diffraction (XRD). The diffraction patterns are recorded at room temperature over a 2θ range of 10°–100°, as shown in Fig. 2, to identify the crystalline phases and evaluate the effect of NiO incorporation on the WO_3 lattice. In the case of pure WO_3 film, the XRD pattern reveals the diffraction peaks centered at 23.88°, 24.77°, 28.65°, 34.36°, 34.83°, 46.35°, 50.03°, and 51.01°. These peaks are assigned to the crystal planes of (002), (020), (111), (−204), (−222),

(−324), (−404), and (−115) respectively and the diffraction pattern confirms the monoclinic structure as predominant.

The WO_3 and NiO combination sample with x = 0.2 wt.% confirmed by diffraction peaks at 24.95°, 29.64°, 34.67°, 56.04° corresponding to (002),(200), (112), and (222) planes.

In the sample with x = 0.4 wt.% NiO, we note the presence of increasingly intensive peak lines at 24.17°, 24.61°, and 29.19°, respectively, with the Miller indices defining the (002), (020), and (112) planes. The slight shift of the peak positions indicates that the NiO incorporation modifies WO3 lattice structure.

The film with the highest NiO content (x = 0.6 wt.%) exhibits diffraction peaks at 24.07°, 24.30°, 28.71°, 33.63°, 43.68°, 55.54°, and 61.87°, which are indexed to the (002), (020), (112), (202), (111), (204), and (304) planes, respectively. The matching with reference cards indicates NiO has been incorporated in the WO_3 lattice. At this concentration, there is a significant change in the peak positions and intensities indicating that lattice distortion is more intense with a tendency to develop multiphase. When excess NiO is added, the incorporation of excess Ni^{2+} ions generates structural defects and induces internal strain, which restrains crystal growth and affects crystallinity. This is the reason for the drop in crystallite size and peak characteristics changes. X'Pert HighScore software and standard JCPDS cards were used to analyze and match all peaks. The films were found to show multiphase characteristics at higher NiO concentration. Moreover, grain size and optical absorption of the 0.6 wt .% sample are consistent with this explanation, indicating composition is relevant for a structural modification and for grain growth, high doping are suitable levels. The mean crystallite size of the films was calculated by using the Debye-Scherrer equation [8].

$$D = 0.94\,\lambda / \beta \cos\theta \qquad (2)$$

In the formula, the diffraction peak's full width at half maximum at the Bragg angle θ is β and X-ray radiation(1.541 Å) wave length is λ. Using this correlation, an approximate crystallite size of 3.9 nm was found for the undoped WO_3 film. These results are consistent with previous reports for WO_3 thin films prepared under analogous conditions [8].

The addition of NiO caused a notable decrease in the crystallite size of WO_3 films. This reduction is attributed to lattice strain introduced by Ni^{2+} ions, which hinder crystal growth, consistent with previous studies on doped WO_3 films [8]. The film thickness was found to be approximately 1.9 nm for 0.4 wt.% NiO film and 1.8 nm for 0.6 wt.% NiO films. This demonstrates that the incorporation of NiO suppresses the growth of WO_3 crystals. The reduction in crystallite size is due to the crystal distortion which is caused because the ionic radius of Ni^{2+} is 0.64 Å and W^{6+} is 0.68 Å. The WO_3 lattice is strained by the smaller Ni^{2+} ions that limit crystal growth and reduce the crystallite size. The calculated structural parameters are summarized in Table 1 [9].

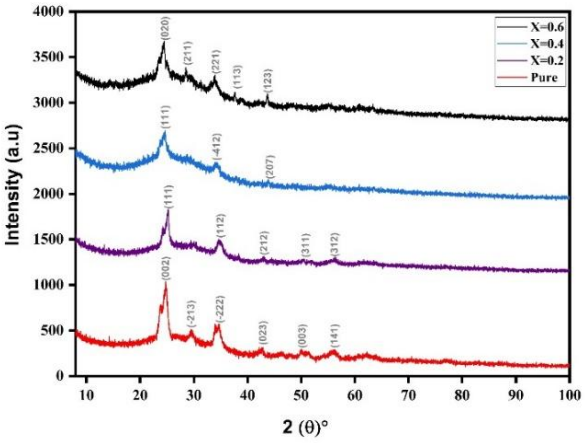

Fig. 2. X-ray diffraction patterns of $(WO3)_{1-x}(NiO)_x$ thin films deposited at room temperature.

3.2. Atomic Force Microscope (AFM)

Atomic force microscopy (AFM) is used to investigate the surface morphology of WO_3 thin films with different NiO concentrations. The films are prepared as $(WO_3)_{1-x}(NiO)_x$ with x = 0.2, 0.4, and 0.6 wt.%. The AFM analysis, as shown in Fig. 3 and Table 2, reveals that the incorporation of NiO significantly affects the grain size and surface roughness of the films. It can be seen that the addition of NiO has pronounced, distinct effects on the film grain size and surface roughness as evidenced in Fig. 3 and Table 2. Moreover, the pure WO_3 film has the highest average grain size, ~99.11 nm, whereas the surface roughness was only moderate (RMS ≈ 11.02 nm). It implies somewhat free crystal development and uniform surface.

With the addition of 0.2 wt.% NiO, the grain size is about 86.66 nm and RMS roughness increases to 22.27 nm. This conduct is consistence with the previous studies and can be explained based on the impairment of crystal growth due to incorporation of Ni [9]. The initial application of NiO disrupts growth and alters the distribution of surface energy.

The original grain size was 53.17 nm while the RMS roughness was 14.43 nm. When the NiO concentration is 0.4 wt.% the grain size further reduced to about 52.11 nm while RMS roughness was reduced to about 14.40 nm. This means improved uniformity on the surface and the beginning of a more ordered nucleation and growth. The film containing 0.6 wt % NiO has the lowest grain size of ~15.21 nm and RMS roughness of ~4.97 nm, which suggests a smooth surface and higher morphological homogeneity. This reduction and smooth surface are in agreement with previous reports on NiO-doped WO_3 films [9], which presented a smoother surface and a more homogenized morphology. The reason for this behavior can be attributed to the addition of NiO, which enhances nucleus density and inhibits grain growth. The lattice distortion and structural defects, as a consequence of the presence of Ni^{2+} ions, restricts the mobility of the adatom during film growth resulting in fine and uniformly distributed grains. The XRD structural changes and enhanced optical absorption of film are in agreement with

the transition to compact and homogeneous surface structures at higher NiO concentrations.

Surface morphology changes are assigned to the lower ionic radii of Ni^{2+} (0.64 Å) and W^{6+} (0.68 Å) in an attempt to create lattice strain and limit grain growth. The observed improvement in surface smoothness and uniformity suggests that NiO-modified WO_3 thin films are suitable candidates for optoelectronic device applications [9].

Table 1. Bragg peak positions and structural parameters of $(WO_3)_{1-x}(NiO)_x$ thin films at different NiO concentrations.

---------- Pure WO_3 ----------				
2θ (°)	d_{hkl} (Å)	FWHM (°)	Crystallite Size (nm)	(hkl)
23.8797	3.72332	1.403	3.9	(002)
24.768	3.59177	0.3775	12.9	(020)
28.6507	3.11323	6.5175	1.2	(111)
34.3611	2.60779	1.3375	6.3	(-204)
34.8349	2.57340	1.7111	4.6	(-222)
46.3497	1.95737	0.2214	43.7	(-324)
50.034	1.82152	0.2104	27.3	(-404)
51.0118	1.78888	0.2466	22.7	(-115)
---------- x = 0.2 wt.% ----------				
2θ (°)	d_{hkl} (Å)	FWHM (°)	Crystallite Size (nm)	(hkl)
24.9468	3.56642	1.2023	4.6	(002)
29.6351	3.01202	5.7864	0.9	(200)
34.6734	2.58501	1.508	3.7	(112)
56.0369	1.63979	1.331	7.3	(222)
---------- x = 0.4 wt.% ----------				
2θ (°)	d_{hkl} (Å)	FWHM (°)	Crystallite Size (nm)	(hkl)
24.1702	3.67922	2.3016	1.9	(002)
24.6109	3.61434	1.0265	4.4	(020)
29.1892	3.05701	8.7892	1.0	(112)
---------- x = 0.6 wt.% ----------				
2θ (°)	d_{hkl} (Å)	FWHM (°)	Crystallite Size (nm)	(hkl)
24.0724	3.69395	2.5615	1.8	(002)
24.3005	3.65979	1.9708	2.3	(020)
28.7136	3.10656	3.7307	1.9	(112)
33.6300	2.66279	2.5287	2.3	(202)
43.6799	2.07061	0.1016	77.9	(111)
55.5449	1.65314	3.1479	2.8	(204)
61.8659	1.49853	5.607	0.9	(304)

3.3. Fourier Transform Infrared (FTIR)

The infrared spectroscopy (FTIR) often used for examination of the chemical bonds and identification of functional groups by their vibrations [10]. The FTIR spectra of $(WO_3)_{1-x}(NiO)_x$thin films recorded in ambient conditions has been displayed in Fig. 4. There is a broad absorption band centered around 3400 cm^{-1} which is assigned to O–H stretching vibrations, indicating the presence of hydroxyl groups on the film surface. This is most likely due to moisture adsorbed on NiO particles. The bending vibration of physically adsorbed water molecules is responsible for the absorption band near 1631 cm^{-1}[11].

Additional absorption bands appearing at approximately 1400 cm^{-1} and 1112 cm^{-1} indicate the presence of carbonate species, while the peak located near 2900 cm^{-1} is assigned to C–H stretching vibrations [12]. The absorption features in the range of 618.84–619.18 cm^{-1} are associated with Ni–O stretching modes, confirming the presence of NiO nanoparticles within the films [13]. Furthermore, a strong absorption band in the range of 700–800 cm^{-1} is attributed to W–O–W bridging vibrations, which confirms the formation of the tungsten oxide lattice structure [14].

3.4. Optical Properties

Optical transmittance (T) measurements are carried out for all deposited thin films, including undoped WO_3 and films containing 0.2, 0.4, and 0.6 wt.% NiO. In addition to transmittance, other optical parameters such as the optical band gap, refractive index, and extinction coefficient are also evaluated. The transmittance spectra of the $(WO_3)_{1-x}(NiO)_x$ thin films, as shown in Fig. 5, are measured at room temperature over the wavelength range of 300–1100 nm.

For all samples, transmittance increases with increasing wavelength. However, the overall transmittance decreases as the NiO content increases. This behavior is attributed to enhanced optical absorption caused by the formation of localized electronic states within the band gap, which

increase the opacity of the films and reduce light transmission.

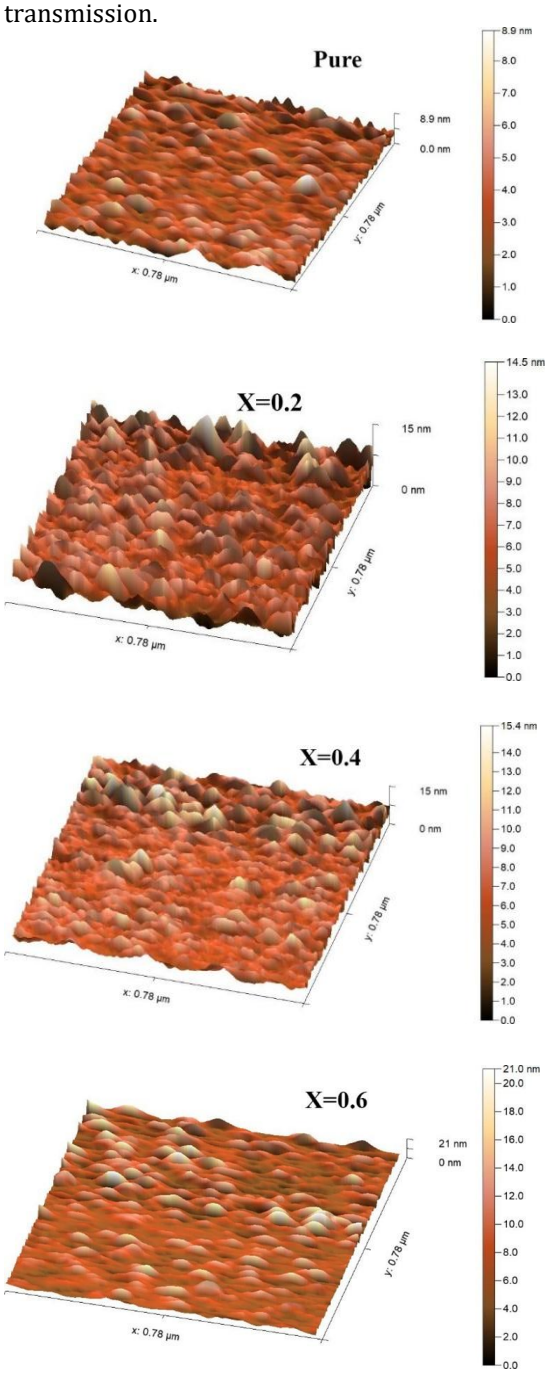

Fig. 3. Topographical AFM images of the thin films showing surface morphology relation with respect to the variation in NiO content (0.2, 0.4, and 0.6 wt.%).

Table 2. The mean surface roughness and average grain size values of thin films at room temperature for different dopant levels of NiO (pure, 0.2, 0.4, and 0.6 wt.%).

Sample	Average Diameter (nm)	RMS roughness (nm)	Average Roughness (nm)
WO_3	99.113	11.02	7.066
$(WO_3)_{1-x}(NiO)_x$ /x=0.2	86.666	22.27	17.150
$(WO_3)_{1-x}(NiO)_x$ /x=0.4	52.118	14.40	12.260
$(WO_3)_{1-x}(NiO)_x$ /x=0.6	15.214	4.966	3.977

The transmittance of pure WO_3 at 500 nm is about 85.59%, and it gradually decreases with NiO addition, reaching approximately 24.39% for the 0.6 wt.% film. This trend is consistent with previous reports, due to increased light absorption caused by defect states and lattice distortion induced by Ni incorporation. At the same time, both absorbance and reflectance increase. The transparency of the films depends on their intrinsic structural and physical properties [15]. Therefore, the observed reduction in transmittance can be directly linked to structural changes in the films induced by NiO incorporation.

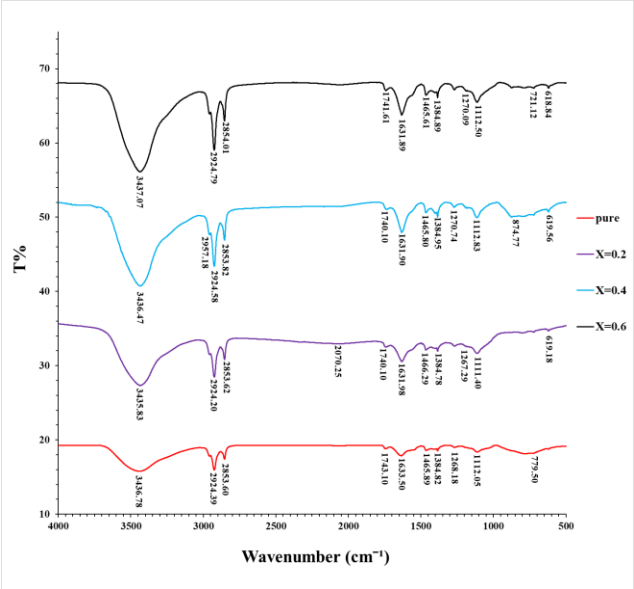

Fig. 4. The FTIR spectra of the prepared $(WO_3)_{1-x}(NiO)_x$ films at room temperature for different NiO weight ratios (0.2, 0.4, and 0.6 wt.%).

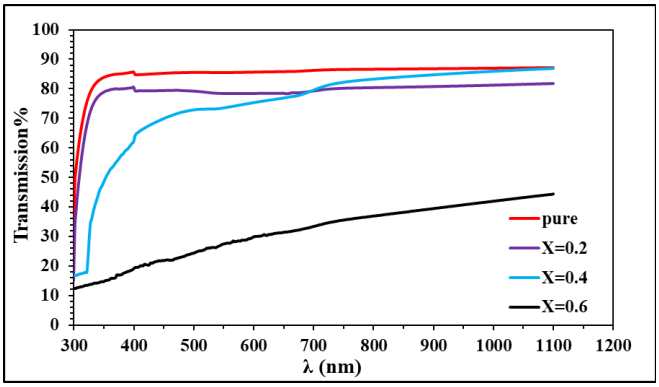

Fig. 5. The change in transmittance with wavelength of the deposited WO_3 film containing NiO at different weight percentages (0.2%, 0.4%, and 0.6%).

The absorption coefficient in the primary absorption edge region of $(WO_3)_{1-x}(NiO)_x$ thin films is calculated based on the absorption data, using Equation (3) [15].

$$I = I_o \exp(-\alpha t) \quad (3)$$

Where Io and I are the incident and the transmitted photon intensity respectively, t is the thickness of the film and α is the absorption coefficient, which is defined as the relative number of the photons absorbed per unit distance of semiconductor, and t is the thickness of the material.

The absorption spectra of films $(WO_3)_{1-x}(NiO)_x$ (Fig. 6) reveal a sharp absorption edge at long wavelengths, while the absorption at short wavelengths ($\alpha > 10^4$ cm^{-1})

subsequently decreases monotonously as λ increases. Due to electronic transitions between energy bands and the density of absorbing centers (impurities, structural defects, etc.), this phenomenon happens. It is observed that an increase in the amount of NiO will increase the absorption coefficient and also reduce the transmittance suggesting better absorption. The films also exhibit compositional and structural changes due to the redshift of the absorption edge, in particular from crystalline to amorphous state of the films. Nickel oxide incorporation into the tungsten trioxide structure enhances the absorption ability of tungsten trioxide in the 300–350 nm wavelength range, and this is very evident [16].

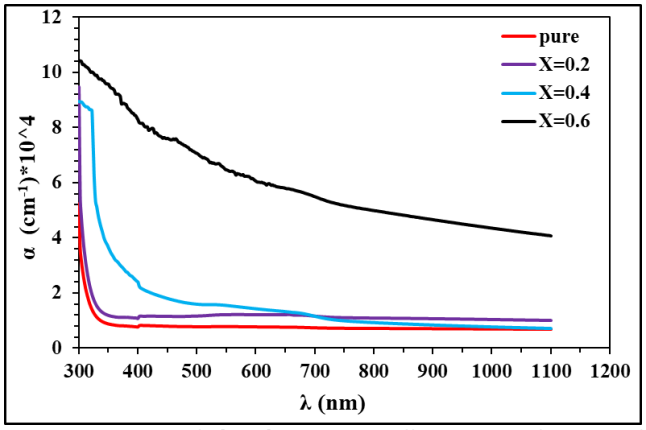

Fig. 6. Variation of the absorption coefficient as a function of wavelength for WO_3 thin films with different NiO loadings (0.2, 0.4, and 0.6 wt.%).

The optical band gap energy (Eg) of the prepared thin films was determined using the absorption coefficient data. The results indicate that all deposited films exhibit a direct optical transition. Therefore, the Tauc method was applied to estimate the direct band gap values. In this analysis, the exponent *r* was taken as 1/2, which corresponds to allowed direct electronic transitions. The optical band gaps were determined and the results were consistent with recent studies on NiO-doped WO_3 thin films [17, 18] by extrapolating the linear region of the (αhν)^r versus photon energy plot to intersect the photon energy axis. The intersection point represents the optical band gap energy [19-21].

$$\alpha h\upsilon = B\,(h\upsilon - Eg)^r \quad (4)$$

In this equation, *Eg* denotes the optical band gap energy, *B* is a material-dependent constant, and *r* is the transition index, which equals 1/2 for allowed direct transitions. The calculated band gap values for the undoped and NiO-doped WO_3 thin films are 3.90, 3.80, 3.75, and 2.60 eV, respectively. All Tauc plots are presented together in Fig. 7 for better comparison. The sharp reduction in band gap for the 0.6 wt.% sample suggests the formation of additional defect levels and possible phase interactions, which enhance electronic transitions and shift the absorption edge toward the visible region.

The significant decrease in band gap energy (Eg) with increasing NiO content is attributed to the incorporation of nickel oxide into the WO_3 crystal structure, leading to the formation of localized electronic states within the restricted band gap. Furthermore, the addition of NiO contributes to increased crystal defects, such as dislocations and stacking defects, which introduce new energy levels within the band gap, thus narrowing the energy gap [22]. As a result, the optical absorption edge shifts toward the visible region of the electromagnetic spectrum, around 375 nm [23]. This reduction in band gap energy is also closely related to the decrease in nanoparticle size. Furthermore, XRD analysis confirms that the changes in crystalline structure are consistent with the observed optical behavior of the prepared thin films [16].

Fig. 8 shows the variation of the refractive index of WO_3 thin films deposited on glass substrates as a function of wavelength for different NiO doping levels in the range of 300–1100 nm. The results show that the refractive index generally decreases as the NiO concentration increases. This behavior can be explained by the narrowing of the optical band gap that occurs when more NiO is incorporated into the WO_3 lattice.

Fig. 9 presents the variation of the extinction coefficient (*k*) for films with different NiO contents over the same wavelength range. Since the extinction coefficient is directly related to the optical absorption of the films, it follows a trend similar to that observed for the optical band gap. Higher absorption corresponds to higher *k* values, particularly in the high-energy region where the optical energy exceeds 4.90 eV. These observations are consistent with the numerical values listed in Table 3.

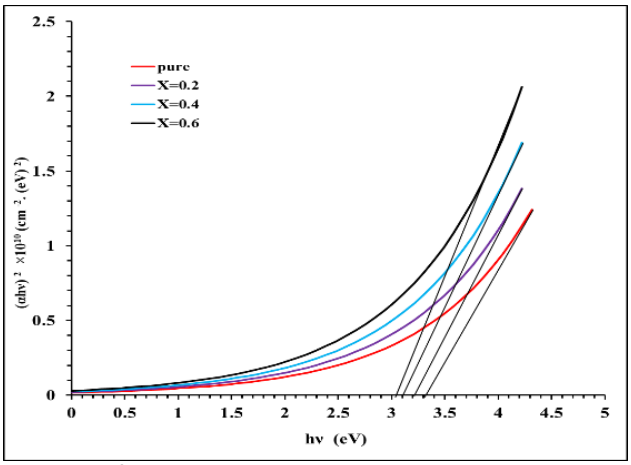

Fig. 7. $(\alpha h\nu)^2$ versus photon energy ($h\nu$) for WO_3 thin films fabricated with varying NiO doping levels (0.2, 0.4, and 0.6 wt.%).

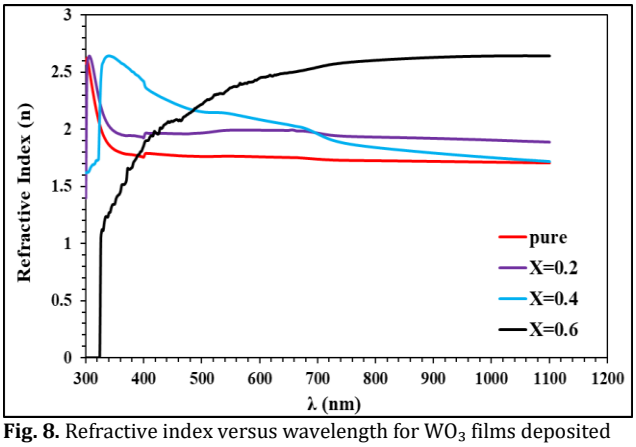

Fig. 8. Refractive index versus wavelength for WO_3 films deposited and doped with different concentrations of NiO (0.2, 0.4, and 0.6 by weight).

Fig.s 10 and 11 show how the dielectric properties of the thin films change with wavelength for NiO contents of 0.2, 0.4, and 0.6 wt.% deposited at room temperature. The real part of the dielectric constant mainly depends on changes in the refractive index of the films. This behavior is consistent with previous reports and is a result of the incorporation of NiO. On the other hand, the imaginary part corresponds to a dielectric energy loss that highly depends on the extinction coefficient.

Since the extinction coefficient is directly related to optical absorption, variations in dielectric loss closely follow the absorption behavior of the films. This relationship is clearly supported by the numerical values listed in Table 3.

Table 3. Optical constants of undoped and NiO-doped WO_3 thin films deposited on glass substrates by pulsed laser deposition, evaluated at a wavelength of λ = 500 nm for different NiO concentrations (0.2, 0.4, and 0.6 wt.%). The corresponding optical band gap values measured at room temperature are also included.

Sample	T(%)	α (cm^{-1})	K	n	ε_r	ε_i	Eg (eV)
WO_3	85.59	7781	0.031	1.765	3.114	0.109	3.30
(WO_3:NiO), X=0.2	79.29	11599	0.046	1.968	3.869	0.182	3.20
(WO_3:NiO), X=0.4	72.81	15866	0.063	2.156	4.643	0.272	3.10
(WO_3:NiO), X=0.6	24.39	70540	0.281	2.219	4.847	1.246	3.00

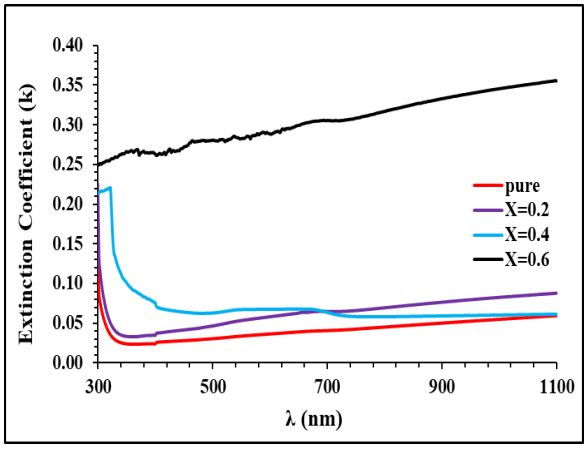

Fig. 9. Extinction coefficient (k) versus wavelength for WO_3 thin films containing different NiO doping levels (0.2, 0.4, and 0.6 wt.%).

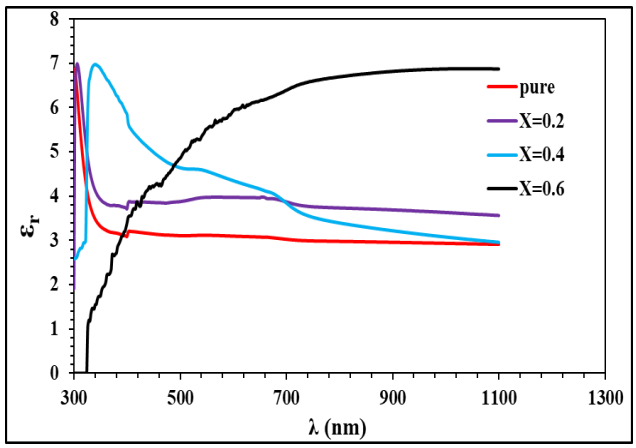

Fig. 10. Variation of the real component of the dielectric constant (ε_r) as a function of wavelength for WO_3 thin films containing different NiO doping levels (0.2, 0.4, and 0.6 wt.%).

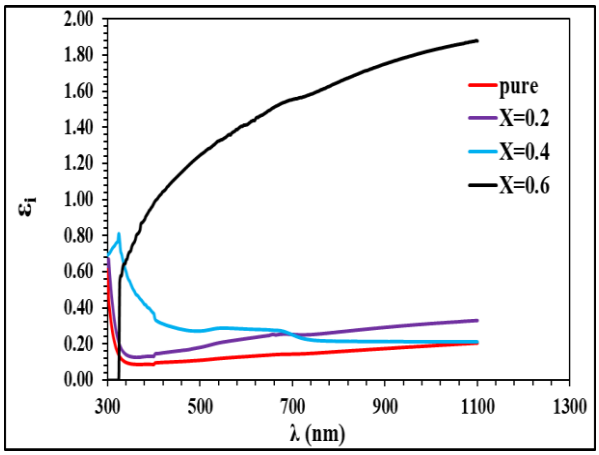

Fig. 11. Dependence of the imaginary component of the dielectric constant (ε_i) on wavelength for WO_3 thin films doped with varying NiO concentrations (0.2, 0.4, and 0.6 wt.%).

4. Conclusions

The NiO-modified WO_3 thin films were deposited on glass by pulsed laser deposition at room temperature with NiO target loadings of 0.2–0.6 wt.%. XRD confirmed monoclinic WO_3 across all samples with composition-dependent changes in peak intensity and apparent crystallite size, while FTIR showed Ni–O vibrational features (~618–619 cm^{-1}) together with characteristic W–O–W modes, supporting successful NiO-related modification of the WO_3 matrix. AFM revealed a systematic refinement of surface morphology with increasing NiO content, where the average grain size decreased from ~99.11 nm (WO_3) to ~15.21 nm (0.6 wt.% NiO) and RMS roughness decreased from ~11.02 nm to ~4.97 nm. Optical measurements showed a strong reduction in transmittance

at 500 nm (85.59% → 24.39%) accompanied by band-gap narrowing (3.30 eV → 3.00 eV), indicating enhanced visible-light absorption with higher NiO content. Overall, controlled NiO addition provides an effective route to tune the structural and optical response of WO_3 films under low-temperature deposition conditions, which is relevant for optoelectronic and light-harvesting applications.

Future work will focus on electrical characterization and device-level performance of the prepared films. Further compositional analysis using EDX or XPS is recommended to confirm the distribution of Ni within the WO_3 matrix.

Acknowledgements

The authors declare that there are no competing financial or personal interests to report which could have influenced the work reported in this paper. The authors also confirm that none of them are currently or have previously served as editor and/or member of the editorial board of the journal to which the manuscript is submitted.

Funding Statement

This research received no specific grant from any funding agency.

Conflicts of Interest

The authors declare that they have no known competing financial interests or personal relationships that could have appeared to influence the work reported in this paper.

Authors Contribution Statement

All authors contributed equally to this work.

References

[1] Aivalioti, C., Androulidaki, M., Tsagaraki, K., Manidakis, E.G., Koliakoudakis, C., Pelekanos, N.T., Modreanu, M. and Aperathitis, E., 2024. Effect of nitrogen co-doping in p-type NiO:Nb thin films on the photovoltaic performance of NiO/TiO_2 transparent solar cells. *Preprints*.

[2] Borca, B. and Bartha, C., 2022. Advances of nanoparticles and thin films. *Coatings*, 12, p.1138.

[3] Gu, X., Lin, S., Qi, K., Yan, Y., Li, R., Popkov, V. and Almjasheva, O., 2024. Application of tungsten oxide and its composites in photocatalysis. *Separation and Purification Technology*.

[4] Hlali, S., Kalboussi, A. and Souifi, A., 2025. Nanomaterials and nanoelectronics: synthesis, properties, and applications for nanotechnology. In: *Nanomaterials and Nanoelectronics*. IntechOpen.

[5] Li, C., Liu, X., Du, X., Yang, T., Li, Q. and Jin, L., 2021. Preparation and optical properties of nanostructure thin films. *Applied Nanoscience*, 11, pp.1967–1976.

[6] Elsevier, 2022. Recent developments in optoelectronic and photonic applications of metal oxides. Elsevier, pp.33–57.

[7] Maktoof, A.Sh. and Mohammed, G.H., 2022. Effect of Au nanoparticles on the structural and optical properties of ($NiO:WO_3$) thin films prepared by PLD technique. *Iraqi Journal of Science*, 63, pp.2502–2513.

[8] Antony, A.J., 2021. Enhancing the visible-light-induced photocatalytic properties of WO_3 nanoparticles by doping with vanadium. *Journal of Physics and Chemistry of Solids*, 157.

[9] Ramkumar, S. and Rajarajan, G., 2017. A comparative study of humidity sensing and photocatalytic applications of pure and nickel-doped WO_3 thin films. *Applied Physics A*, 123, p.401.

[10] Atul, A.K., 2022. Synthesis and characterization of NiO nanoparticles by chemical co-precipitation method: an easy and cost-effective approach. *Brazilian Journal of Physics*, 52.

[11] Rahdar, A., Aliahmad, M. and Azizi, Y., 2015. NiO nanoparticles: synthesis and characterization. *Journal of Nanostructures*, 5, pp.145–151.

[12] Hassan, A.I., Khawla, S., Khashan, J.A. and Saimon, 2014. Preparation and characterization of NiO thin films by pulsed laser deposition. *Engineering and Technology Journal*, 33.

[13] Krašovec, U.O., Vuk, A. and Orel, B., 2001. IR spectroscopic studies of charged–discharged crystalline WO_3 films. *Electrochimica Acta*, 46, pp.1921–1929.

[14] Kasap, S., 2002. Principles of electronic materials and devices. *IEEE Electrical Insulation Magazine*, 18.

[15] Al-Ogaili, H. and Hathot, S., 2023. Photo-sensitive electrodes based on $NiO:SnO_2$ nanocomposites prepared by chemical method. *Digest Journal of Nanomaterials and Biostructures*, 18.

[16] Gholizadeh, Z. et al., 2024. Novel boehmite and η-alumina nanostructures synthesized using a green ultrasonic-assisted hydrothermal method by clove extract for water treatment. *Journal of Water Process Engineering*, 65, p.105786.

[17] Gholizadeh, Z. et al., 2026. The novel alumina/CQDs nanocomposites for modifying optical and structural properties of alumina nanostructure. *Scientific Reports*.

[18] Mbamara, C., Nworie, I.C., Brown, N.O., Otah, P.B., Oko, K.I., Idu, H.K. and Amadi, M.C., 2024. Synthesis and characterization of nickel-doped cerium oxide thin films using solution growth technique. *Nigerian Journal of Physics*, 33, pp.139–146.

[19] Fakhri, M.A., 2016. Annealing effects on opto-electronic properties of Ag_2O films grown using thermal evaporation techniques. *International Journal of Nanoelectronics and Materials*, 9, pp.93–102.

[20] Salim, E.T., Awayiz, M.T. and Mahdi, R.O., 2019. Tea concentration effect on the optical, structural, and surface roughness of Ag_2O thin films. *Digest Journal of Nanomaterials and Biostructures*, 14, pp.1151–1159.

[21] Chang, X. et al., 2011. Synthesis of transition metal-doped tungsten oxide nanostructures and their optical properties. *Materials Letters*, 65(11), pp.1710–1712.

[22] Hameed, M.A., Ali, O.A. and Al-Awadi, S.S., 2020. Optical properties of Ag-doped nickel oxide thin films prepared by pulsed-laser deposition technique. *Optik*, 206.